Journal of Electromagnetic Waves and Applications

Publication details, including instructions for authors and subscription information:
http://www.tandfonline.com/loi/tewa20

Full-wave FEM simulations of electromagnetic waves in strongly magnetized non-homogeneous plasma

G. Torrisi[ab], D. Mascali[a], G. Sorbello[ac], L. Neri[a], L. Celona[a], G. Castro[a], T. Isernia[b] & S. Gammino[a]

[a] INFN - Laboratori Nazionali del Sud, 62 via S. Sofia, 95125 Catania, Italy.

[b] Dipartimento di Ingegneria dell'Informazione, delle Infrastrutture e dell'Energia Sostenibile (DIIES), Universitá Mediterranea di Reggio Calabria, Via Graziella, I-89100 Reggio Calabria, Italy.

[c] Dipartimento di Ingegneria Elettrica Elettronica ed Informatica, Universitá degli Studi di Catania, Viale Andrea Doria 6, 95125 Catania, Italy.

Published online: 04 Apr 2014.

To cite this article: G. Torrisi, D. Mascali, G. Sorbello, L. Neri, L. Celona, G. Castro, T. Isernia & S. Gammino (2014) Full-wave FEM simulations of electromagnetic waves in strongly magnetized non-homogeneous plasma, Journal of Electromagnetic Waves and Applications, 28:9, 1085-1099, DOI: 10.1080/09205071.2014.905245

To link to this article: http://dx.doi.org/10.1080/09205071.2014.905245

Journal of Electromagnetic Waves and Applications, 2014
Vol. 28, No. 9, 1085–1099, http://dx.doi.org/10.1080/09205071.2014.905245

Full-wave FEM simulations of electromagnetic waves in strongly magnetized non-homogeneous plasma

G. Torrisi[a,b*], D. Mascali[a], G. Sorbello[a,c], L. Neri[a], L. Celona[a], G. Castro[a], T. Isernia[b] and S. Gammino[a]

[a]*INFN – Laboratori Nazionali del Sud, 62 via S. Sofia, 95125 Catania, Italy;* [b]*Dipartimento di Ingegneria dell'Informazione, delle Infrastrutture e dell'Energia Sostenibile (DIIES), Universitá Mediterranea di Reggio Calabria, Via Graziella, I-89100 Reggio Calabria, Italy;* [c]*Dipartimento di Ingegneria Elettrica Elettronica ed Informatica, Universitá degli Studi di Catania, Viale Andrea Doria 6, 95125 Catania, Italy*

(*Received 10 December 2013; accepted 10 March 2014*)

Electromagnetic wave propagation in anisotropic media has been widely studied over the last decades since there are several applications where anisotropy plays an important role. This paper presents a procedure to carry out three-dimensional (3D) finite element method (FEM) full-wave simulations of the electromagnetic field in inhomogeneous magnetized plasma of an electron cyclotron resonance ion source (ECRIS). We used COMSOL Multiphysics® software and MATLAB® to model a cold anisotropic magnetized plasma, described by full-3D non-uniform dielectric tensor, enclosed by the metallic cylindrical cavity where the plasma is formed. A proper mesh generation, exploiting FEM-based COMSOL versatility, allowed us to optimally model ECRIS cavity and microwave waveguide launching structure, with a good computational efficiency and high resolution of the solution especially around the resonance regions. Numerical simulations have been performed in the frequency domain: in the resonance regions especially, the material properties exhibit a spatial variation that leads to a large sparse ill-conditioned matrix which is solved by MUltifrontal Massively Parallel Solver (MUMPS) direct method. We implement a method to perform full-wave simulations considering a cold plasma model for the constitutive relations; the obtained results show that the presence of ECR layer, along with the cavity walls, strongly influences the shape and strength of the electromagnetic field distribution, featuring a strong non-uniformity of the main electromagnetic parameters.

Keywords: FEM; ECRIS; modeling; plasma; electromagnetic wave

1. Introduction

A new approach is argued – based on a three-dimensional (3D) finite element methods (FEM) electromagnetic simulations by using COMSOL Multiphysics and MATLAB to solve wave propagation in an inhomogeneous anisotropic cold plasma considering a position-dependent non-axial magnetic field – in order to explore in more detail the problem of RF energy deposition in microwave-generated linear plasmas confined by non-axisymmetric magnetostatic fields, under unfavorable conditions of small vessel-size-over-wavelength ratio. In these small devices, where the typical dimension are often comparable with wavelength of the injected RF wave, the effects of the vessel walls cannot be neglected (i.e. the waves cannot be assumed as plane waves propagating in free space)

*Corresponding author. Email: peppetorrisi@lns.infn.it

and a full-wave calculation including multireflections and "cavity scrambling" effects must be invoked. This represents a significative step forward with respect to other approaches already attempted in the past.[1]

The propagation of waves in anisotropic media is relevant for many fields of optics and microwaves. Searching the solution of Maxwell's equations, by considering a metallic cylindrical cavity eventually, completely or partially filled by an anisotropic material whose electric permittivity is described by a second-order tensor, is a particularly difficult task. In electromagnetism, only very few scenarios can be analytically solved. In the present case, the cavity has a non-canonical form, and is filled by a non-homogeneous anisotropic medium (magnetized plasma); therefore, the numerical approach is mandatory. Such is the case of electron cyclotron resonance ion sources (ECRIS) [2] plasma chamber. These devices produce multicharged ions extracted by a plasma heated by microwaves. Several experimental results show that electromagnetic waves coupling with the plasma load is crucial to optimally transfer energy to the electrons, then to optimize plasma ionization and ion beam extraction.[3–5] However, for a better understanding of the physical processes involved in plasma and in beam formation process, it is crucial to consider the actual geometry of ECRIS microwave injection in presence of a realistic plasma model. Up to now, several studies make various approximations by considering the medium as an equivalent dielectric load [6] and by solving the wave equation in Wentzel Kramers Brillouin (WKB) approximation.[7] This latter approximation is questionable in particular regions of the plasma, where cut-offs and resonances break the slow-varying assumptions of the media parameters $\left|\frac{\nabla\cdot\vec{k}}{k^2}\right| \ll 1$, and a fortiori it is not feasible in ECRIS configuration where plasma load and the chamber's electromagnetic properties are extremely variable even over fractions of a wavelength. In these cases, a full wave solution of Maxwell's equations is needed. This paper presents a new full wave simulation model in which Maxwell's equations are solved by using COMSOL Multiphysics FEM solver whose input parameters are provided by a dedicated software running in MATLAB. We exploit COMSOL's ability to accept 3D space-varying dielectric tensor (computed in Matlab) and to solve wave equation in the inhomogeneous, anisotropic, and lossy plasma produced in the multimode ECRIS cavity, taking into account a realistic electron density and the so-called B-min magnetic field confining the plasma.[2] The simulations include energy absorption by the plasma and the presence of lossy cavity walls.

2. Electromagnetic formulation of wave equation in plasma

Under the influence of a magnetic field, a plasma exhibits an anisotropic electric behavior and can be modeled introducing anisotropic constitutive relations where the permittivity is a second-order tensor. Considering the plasma as a dispersive medium modeled as a cold magnetofluid with collisions,[8] Maxwell's equations and constitutive relation for source-free, anisotropic media, using harmonic time dependence $e^{j\omega t}$, can be written as:

$$\nabla \times \vec{E}(\vec{r}) = -j\omega\vec{B}(\vec{r}) \tag{1a}$$

$$\nabla \times \vec{H}(\vec{r}) = j\omega\epsilon_0\vec{E}(\vec{r}) + \vec{J}(\vec{r}) = j\omega\overline{\overline{\epsilon}}\cdot\vec{E} \tag{1b}$$

where

$$\vec{J} = \overline{\overline{\sigma}}\vec{E} \tag{2a}$$

and

$$\overline{\overline{\epsilon}}\cdot\vec{E} = \epsilon_0\vec{E} + \frac{\vec{J}}{j\omega} = \left(\epsilon_0 + \frac{\overline{\overline{\sigma}}}{j\omega}\right)\cdot\vec{E} \tag{2b}$$

Displacement $j\omega\epsilon_0\vec{E}(\vec{r})$, and conduction $\vec{J}(\vec{r})$ currents are collected in a tensorial term describing the field–plasma interaction introducing the dielectric tensor:

$$\overline{\overline{\epsilon}} = \epsilon_0 \left(\overline{\overline{I}} - \frac{j\overline{\overline{\sigma}}}{\omega\epsilon_0} \right) \tag{3}$$

Eliminating the magnetic field between (1a) and (1b) and using constitutive relations, we obtain the wave equation:

$$\nabla \times \nabla \times \vec{E} - \frac{\omega^2}{c^2}\overline{\overline{\epsilon_r}} \cdot \vec{E} = 0 \tag{4}$$

The above Equation (4) can be solved as a driven problem by a FEM solver that supports a non-homogeneous tensorial constitutive relation; in the present work, we used COMSOL and an external MATLAB routine.

2.1. Dielectric tensor formulation

To model the plasma response in the GHz range frequencies, we describe the anisotropic behavior in terms of a dielectric tensor $\overline{\overline{\epsilon}}$ following the "cold plasma" model.[1] However, in [8], wave Equation (4) is analyzed in free space for plane wave and the dielectric tensor $\overline{\overline{\epsilon}}$ is derived by assuming the applied magnetic field aligned to one of the coordinate axes (tipically, z-axis).[9] This assumption does not cause loss of generality in most of cases where $B_{0_x}, B_{0_y} \ll B_{0_z}$, but not in ECRIS because the magnetic field structure is obtained by a superimposition of solenoidal and hexapolar coils creating a "quasi-axisymmetric" non-uniform magnetostatic field, called "B-min" structure.

Consequently, to obtain a general valid solution, it is essential that constitutive parameters are formulated in a general orthogonal Cartesian coordinate system.

In cold plasma approximation,[8] the determination of $\overline{\overline{\epsilon}}$ is based on the equation of motion for single particle:

$$(-j\omega + \omega_{\text{eff}})\vec{v} + \frac{e}{m_e}\vec{B}_0 \times \vec{v} = \frac{e}{m_e}\vec{E} \tag{5}$$

Solving (5) in $\vec{v}$ and using the constitutive relation:

$$\vec{J} = N_0 q \vec{v} = \overline{\overline{\sigma}} \cdot \vec{E} \tag{6}$$

we can obtain $\overline{\overline{\sigma}}$ that is related to $\overline{\overline{\epsilon}}$ as we can see in (1b) and (2b).

Finally, $\overline{\overline{\epsilon}}$ is:

$$\begin{aligned}\overline{\overline{\epsilon}} = \epsilon_0\overline{\overline{\epsilon}}_r &= \epsilon_0\left(\overline{\overline{\epsilon'}} - j\overline{\overline{\epsilon''}}\right) = \epsilon_0\left(\overline{\overline{I}} - \frac{j\overline{\overline{\sigma}}}{\omega\epsilon_0}\right) \\ &= \epsilon_0 \begin{bmatrix} 1 + j\frac{\omega_p^2}{\omega}\frac{a_x}{\Delta} & j\frac{\omega_p^2}{\omega}\frac{c_z + d_{xy}}{\Delta} & j\frac{\omega_p^2}{\omega}\frac{-c_y + d_{xz}}{\Delta} \\ j\frac{\omega_p^2}{\omega}\frac{-c_z + d_{xy}}{\Delta} & 1 + \frac{j\omega_p^2}{\omega}\frac{a_y}{\Delta} & j\frac{\omega_p^2}{\omega}\frac{c_x + d_{yz}}{\Delta} \\ j\frac{\omega_p^2}{\omega}\frac{c_y + d_{xz}}{\Delta} & j\frac{\omega_p^2}{\omega}\frac{-c_x + d_{zy}}{\Delta} & 1 + j\frac{\omega_p^2}{\omega}\frac{a_z}{\Delta} \end{bmatrix}\end{aligned} \tag{7}$$

where $a_m = (-\mathrm{j}\omega + \omega_{\mathrm{eff}})^2 + B_{0_m}^2 \left(\frac{e}{m_e}\right)^2$, $c_m = B_{0_m}\left(\frac{e}{m_e}\right)(-\mathrm{j}\omega + \omega_{\mathrm{eff}})$, $d_{mn} = B_{0_m} B_{0_n}\left(\frac{e}{m_e}\right)^2$ with $m = x, y, z, n = x, y, z$ and

$$\Delta = (-\mathrm{j}\omega + \omega_{\mathrm{eff}})a_x + B_{0_z}\left(\frac{e}{m_e}\right)(c_z - d_{xy}) + B_{0_y}\left(\frac{e}{m_e}\right)(c_y + d_{xz}).$$

$\overline{\overline{\epsilon}}'$ is the real part of relative permittivity $\overline{\overline{\epsilon}}_r$, $\overline{\overline{\epsilon}}''$ is the imaginary part, ω is the angular frequency of the microwave, $\omega_p = \sqrt{\frac{n_e e^2}{m_e \epsilon_0}}$ is the plasma oscillation angular frequency, n_e is the electron density, m_e is the electron mass, e is the electron charge, j is the imaginary unit and ω_{eff} is the collision frequency; the latter accounts for the collision friction (thus modeling wave damping) and resolves the singularity of some elements of (7).

At the electron cyclotron resonance (ECR) layer, where $|B_0(x, y, z)| = B_{ECR}$ and $\omega_c = \frac{eB_0}{m_e} = \omega$, Δ becomes very small, resulting in an strong variation of $\overline{\overline{\epsilon}}_r$. Depending on the values of ω, ω_p and ω_{eff}, $\overline{\overline{\epsilon}}$ and the correlated wave vector $k = k_{real} - \mathrm{j}k_{im}$ can have real or imaginary part; therefore, different wave propagation or attenuation scenarios are possible.

In [1], authors investigate only some specific scenarios, since the anisotropic plasma is approximated by an isotropic dielectric with the refractive index of R-wave.[10] This can be done only for plane wave with a precise polarization and a fixed angle between $\vec{k}$ and $\vec{B}_0$ that allows to replace the tensor (7) with a scalar quantity, i.e. the refraction index of either ordinary or extraordinary waves that can be analytically computed.

Our quite general formulation, which considers only the cold-plasma electromagnetic modes, (not the ion sound and electrostatic waves coming from the hot plasma approximation), allows us to consider in 3D simulations the full tensorial properties of the magnetized plasma we are dealing with, evaluating the plasma response on electromagnetic wave propagating inside ECRIS cavity. In the following, we do not consider any particular propagation mode or a specific angle between $\vec{k}$ and $\vec{B}_0$, taking into account any multiple scattering of the waves at chamber walls and considering arbitrary propagation angle at whatever point into the plasma.

3. Numerical simulations

3.1. Model definition

The cylindrical cavity representing the plasma chamber is a metallic box connected to a microwave source via a rectangular waveguide operating in the TE_{10} mode. Figure 1 shows the geometry and in Table 1,[2] all the important simulation input parameters are listed. Many geometrical details of ECRIS assembly can be removed in order to reduce the computational cost of the simulations without any loss in the approach validity.

The inner cavity volume is filled by lossy plasma characterized by dielectric tensor (7). The lossy cavity walls are modeled via the appropriate "impedance boundary condition." [11] The magnetostatic field can be modeled in a 3D environment according to the following equations: $B_{0_x} = x(-B_1 z + 2S_{ex} y)$, $B_{0_y} = -B_1 yz + S_{ex}(x^2 - y^2)$, $B_z = B_1 z^2 + B_2$, where S_{ex} is a constant related to the hexapole field, and B_1 and B_2 are related to the solenoid ones. Figure 2 displays the electron density n_e and magnetostatic profile $\vec{B}_0$ along the line ($x = 0$, $y = 0, z$), used as simulation input parameters, in the normalized form: $X = \frac{\omega_p^2}{\omega^2} = \frac{n_e e^2}{m_e \epsilon_0}\frac{1}{\omega^2}$, $Y = \frac{\omega_c}{\omega} = \frac{e|B_0|}{m_e}\frac{1}{\omega}$. Absolute values of n_e profile are shown in the right-hand vertical axis of Figure 3. The density profile comes from modeling on plasma dynamics and heating

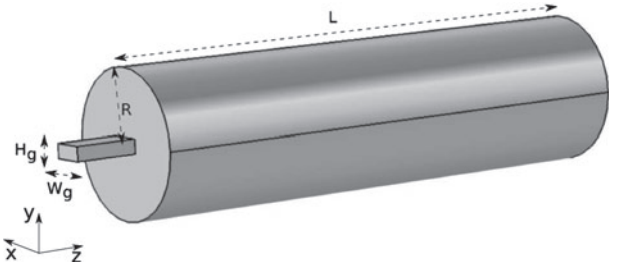

Figure 1. Simulated geometry: cavity and waveguide.

Table 1. Simulation input parameters.

Parameter	Value	Description
L	480 (mm)	Cavity length
R	65 (mm)	Cavity radius
ν_{RF}	8 (GHz)	Frequency
ω_{RF}	$2\pi\nu_{RF}$ (rad / s)	Angular frequency
ω_{eff}	$\omega_{RF}/10^3$ (rad / s)	Collision frequency
W_g	28.5 (mm)	Waveguide width
H_g	12.6 (mm)	Waveguide height
P_{RF}	100 (W)	RF Power

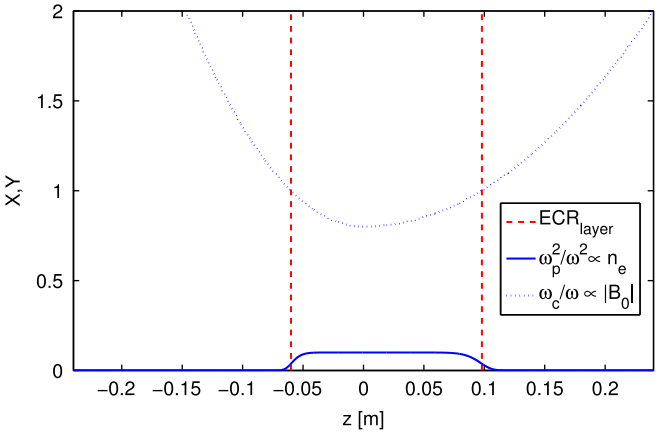

Figure 2. Profiles of $X = \omega_p^2/\omega^2$ (proportional to n_e) and $Y = \omega_c/\omega$ (proportional to B_0) along the longitudinal z-axis, used as input parameters to compute the permittivity tensor for 3D simulation. The dash vertical lines highlight the ECR layer positions.

in [12]: the plasma density distribution into an ECRIS splits into two different regions: (i) a dense volume enclosed by the iso-magnetic surface corresponding to ECR condition (and called "plasmoid") and (ii) a rarefied halo made of particles escaping or flowing out from the plasmoid. Then we used an electron density "Gaussian" profile showing a flat top shape into the plasmoid and a rapid decrease from ECR layers towards the plasma chamber walls. We started by setting as maximum density, located at the center of the chamber ($z = 0$),

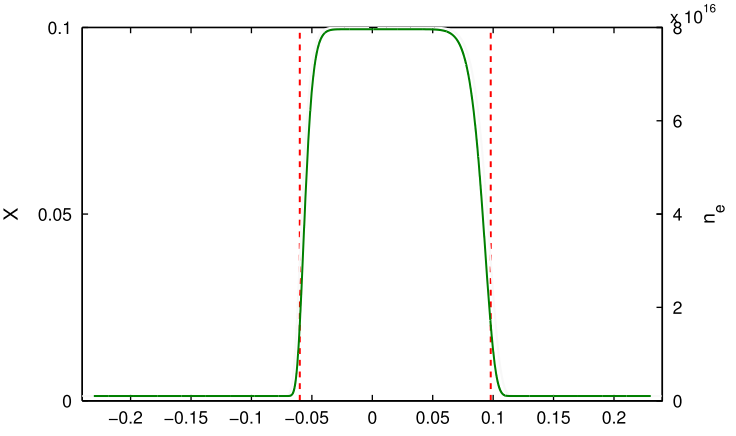

Figure 3. Zoom of the profiles of $X = \omega_p^2/\omega^2$ (proportional to n_e) and (on the right) n_e along the longitudinal z-axis, used as input parameters to compute the permittivity tensor for 3D simulation. The dash vertical lines highlight the ECR layer positions.

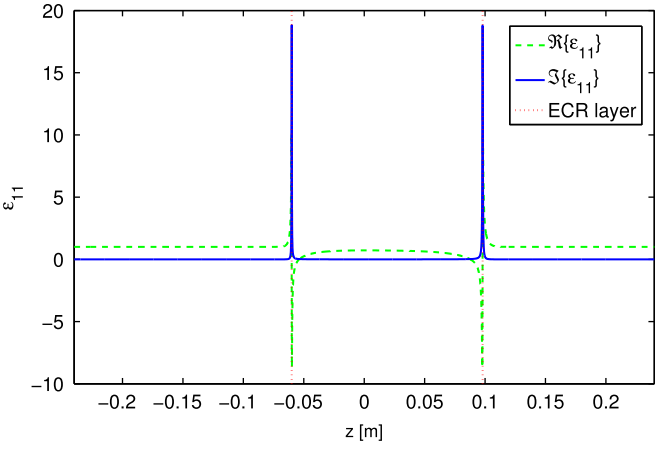

Figure 4. Real and Imaginary part of ϵ_{11}: they are peaked at ECR layer.

$n_{max} = 0.1 n_c$ where $n_c = \frac{\omega^2 \epsilon_0 m_e}{e^2}$ is the cut-off density of the ordinary wave.[8] These data allow to compute in MatLab environment, the full anisotropic tensor $\overline{\overline{\epsilon}}(x, y, z)$, whose $\overline{\overline{\epsilon}}_{11}$ element is plotted for sake of example along z-axis in Figure 4. The problem is finally solved in two stages: first, we compute in MatLab environment the full anisotropic tensor (7), then the wave equation is solved by using the direct linear system solver MUMPS [13] of COMSOL.

3.2. *Mesh generation*

Mesh creation procedure is a critical issue for a FEM simulation: it significantly impacts on rate of convergence, solution accuracy, and CPU time required. The geometry and physics problem require an unstructured tetrahedrical mesh and a mesh density high enough to

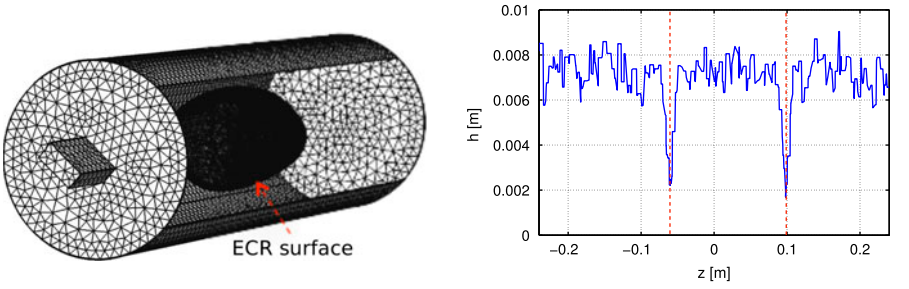

(a) Non-uniform mesh density accounting for ECR layer.

(b) Mesh element size h along longitudinal z-axis. The dash vertical lines highlight the ECR layer positions.

Figure 5. Mesh generated in COMSOL.

capture all relevant electromagnetic features, especially in ECR zone where $|B_0(x, y, z)| = B_{ECR}$ and, in a very thin layer, dielectric permittivity changes very rapidly (see Figure 4). This implies a non-uniform mesh density that has to strongly increase around the ECR layer. In our case, this was done by individuating the iso-surface $|B_0(x, y, z)| = B_{ECR}$ (that can be computed and reproduced in COMSOL) working as a reference surface for starting mesh construction and growth. The mesh size is kept very small close to this surface, and grows with a controllable rate to keep as low as possible the computational costs. COMSOL mesh generation flexibility allowed to obtain a very high mesh quality even though we addressed a critical problem with non-smooth surfaces potentially leading to tetrahedrons with poor aspect ratio. Figure 5(a) shows spatial distribution of the mesh size, which becomes very small around the ECR closed surface where the refractive index is subjected to very large oscillations. Figure 5(b) shows the absolute size of the tetrahedrons along the longitudinal z-axis.

3.3. Computational issues

Considering the valuable amount and the importance of the results provided by the simulation, we put several efforts to check computational accuracy and the convergence of the chosen mesh refinement strategy. FEM solution of the electromagnetic problem of waves propagating into an anisotropic medium (the magnetized plasma) is a very difficult computational effort especially because of the strong fluctuation in the refractive index. Despite the mesh strategy discussed in Section 3.2, the setup leads to very ill-conditioned linear, sparse, complex, non-symmetric systems. To avoid convergence problems and slow convergence rate, we used direct COMSOL sparse linear system solver MUMPS,[13] solving models with more than 4 million of unknowns with the aid of a computer equipped of four 2.70 GHz eight-core Intel® Xeon® E5-4650 Processors, with 256 GB of RAM. Usually, the standard convergence criterion adopted by commercially available simulators implements an adaptive mesh refinement that is based on the evaluation of the solution's error between two consecutive passes. This philosophy is not applicable in a direct resolution scenario which does not require iterations and does not include convergence criteria (only round-off error checks). We were therefore forced to individuate a proper mesh refinement criterion; the electromagnetic power loss density P_{loss} was individuated as a physically most significant parameter that, as shown in the previous pages, critically depends on the wave dynamics in near resonance zones where k, $\overline{\overline{\epsilon}}$ and $\vec{E}$ strongly fluctuate and the mesh size accuracy is of particular relevance. This parameter was evaluated for simulations with different mesh densities in order to make sure that results are mesh independent. In Table 2,

Table 2. Summary of results: simulations performed on 4 eight-core Intel® Xeon® 2.70 GHz E5-4650 Processors, 256 GB RAM.

Maximum element size	No. of tetrahedra	DoF	CPU time	RAM (GB)	Power loss (Watt)
$\lambda/4$	407473	2.58e^6	51 min, 24 s	129	73.43 W
$\lambda/5$	430200	2.73e^6	1 h, 6 min	133	72.94 W
$\lambda/7$	520031	3.31e^6	1 h, 12 min	158	72.80 W
$\lambda/8$	597284	3.80e^6	2 h, 2 min	193	72.51 W

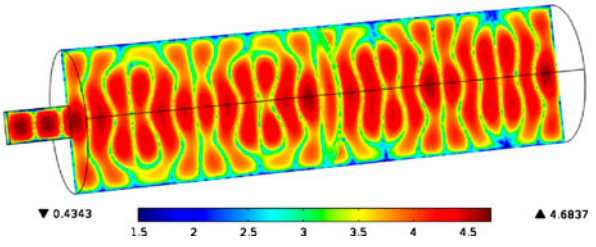

Figure 6. $\log_{10}(|E|+1)$ in vacuum chamber (false color representation).

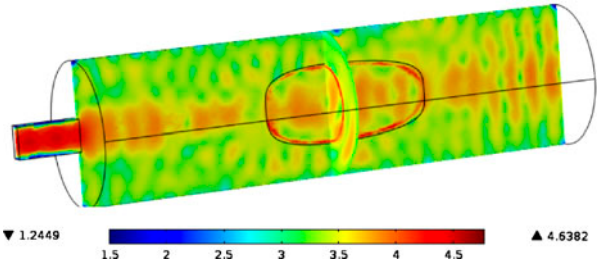

Figure 7. $\log_{10}(|E|+1)$ in plasma-filled chamber (false color representation).

different mesh setups are shown: five mesh elements per wavelength[3] are sufficient to obtain a convergent P_{loss}, whose value varies less than 0.4%.

3.4. Simulation results

Hereinafter, we show the most important simulation results. It is noticeable how the typical standing wave pattern of a vacuum resonating cavity, (Figure 6), is strongly perturbed when the plasma-filled cavity is considered (Figure 7). Moreover, we can clearly see in Figures 7 and 8 that, when electromagnetic wave approaches the resonance zones, the electric field increases up to almost one order of magnitude. On the other hand, an attenuation of electric field on z-axis (Figure 9) is present, as already seen in [12] for electron density distribution that shows a "hole" in near axis zone, due to electromagnetic field distribution pattern.

In addition, on the resonance surface the imaginary part of wave vector k_{im}, (see Figure 10), is peaked and the microwave power is damped because the electric field decreases as $e^{k_{im}r}$; in these zones, the dissipated power density, shown in Figure 10, achieves its maximum value. In Figure 11, we show the dissipated power density by multislice

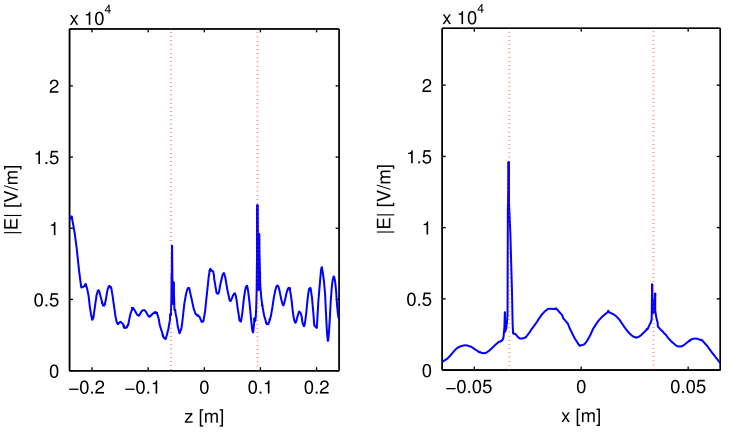

Figure 8. Electric field on a off-axis longitudinal line ($x = 0.01$, $y = 0$, z), parallel to z-axis, and along the transversal direction x (x, 0, 0). The red dot lines highlight the ECR layer positions.

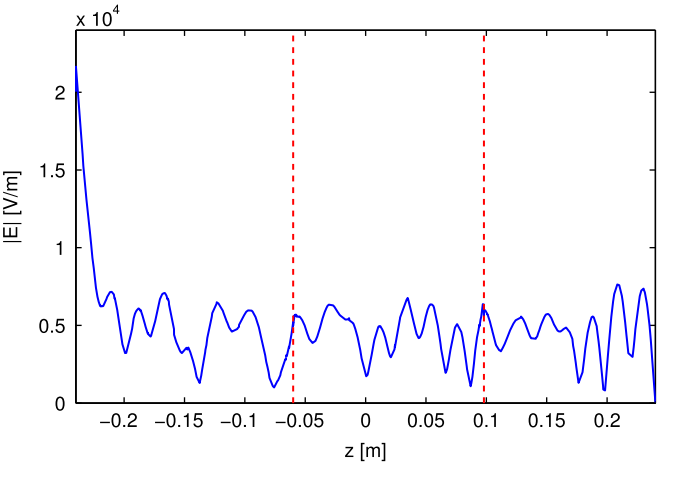

Figure 9. Electric field along z-axis ($x = 0$, $y = 0$, z). The red dot lines highlight the ECR layer positions.

representation (3D): it is evident that the most part of the power is absorbed at the ECR layer. At the frequency of 8 GHz, the 95% of input RF Power is absorbed from lossy plasma and only the 0.3% is dissipated from copper cavity walls. The other relevant result is that the electromagnetic field is not uniformly distributed on ECR surface and it produces a non-uniform power loss density distribution on ECR surface as it can be seen in Figure 12. This result is consistent with the experimental results and the plasma modeling [14] suggesting that the RF energy is not uniformly deposited inside the plasma core, being affected by quasi-modal structures established in the plasma-filled cavity. As a general comment, the above-presented results are in agreement with theory and represent an important step forward in ECRIS plasma comprehension with respect to older studies.[9]

The model versatility allows to solve and evaluate the effects on electromagnetic field propagation and absorption by using different ion source operating parameters, as different electron density n_e profiles (see Figure 13), while keeping a Gaussian profile in all simulations. This parametric study has been done for an ECRIS cavity operating at 5 GHz: at this operating point, the computation time decreases.

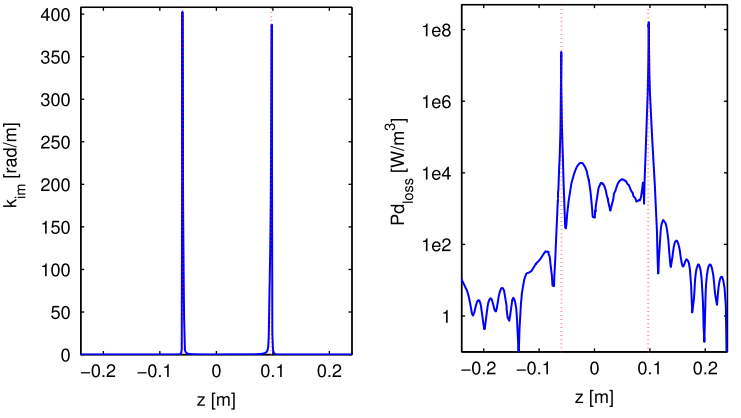

Figure 10. k_{im} and power loss density Pd_{loss} along z-axis. At ECR layers(red dot lines) k_{im} and Pd_{loss} show a maximum.

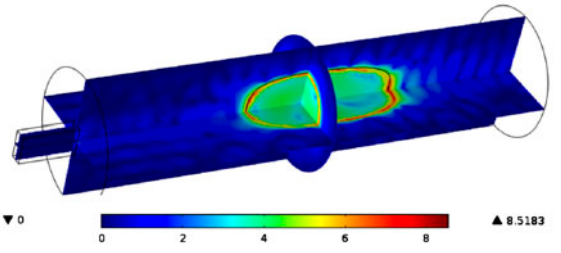

Figure 11. Electromagnetic power loss density (W/m^3) (logarithmic scale).

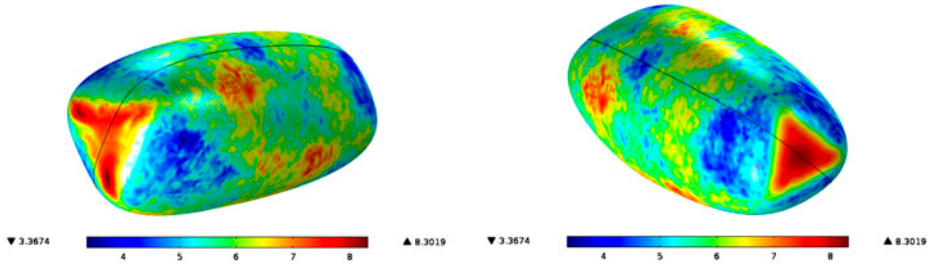

(a) Electromagnetic power loss density (W/m^3) on ECR surface (left side view)

(b) Electromagnetic power loss density (W/m^3) on ECR surface (right side view)

Figure 12. Non-uniform distribution of electromagnetic power loss density on ECR surface.

In Figure 14, the electric field on the z-axis when simulating the different n_e profiles is shown. Thereinafter, they will be labeled then as #1–#4 (for, respectively, $\frac{max(n_e)}{n_c} = 0.1$, 0.5, 0.9, and 1.2).

Two results are more relevant in Figure 14: (a) for the #3 profile there is a "cavity effect" and a field amplification in the inner plasmoid region (plasma resonant effect) ascribable to the discontinuity at ECR layers, that is very similar to what has been observed in [9] in a simpler configuration, and (b) when $n_e > n_c$ (#4 profile)[4], the wave still propagates into the plasmoid without appreciable attenuation. In the case #3, inside the plasmoid k_{real}

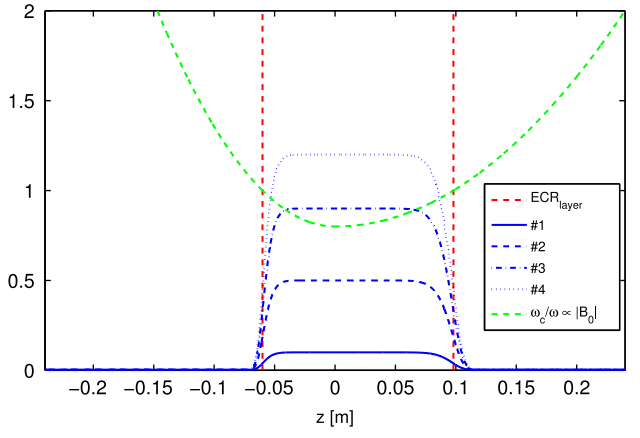

Figure 13. Different n_e profiles used for simulations.

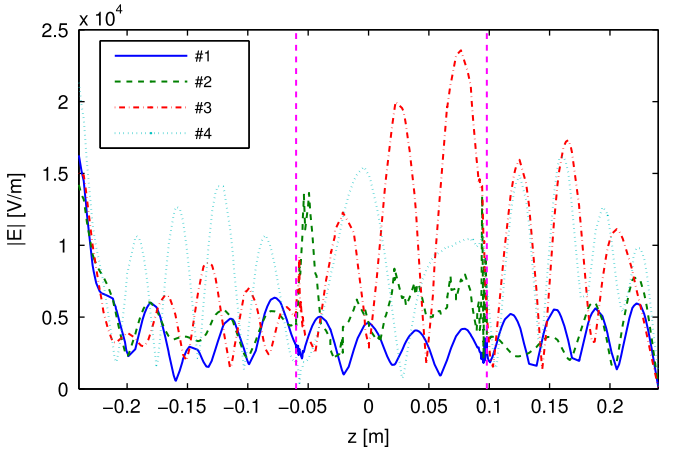

Figure 14. Electric field along z-axis for different density profiles.

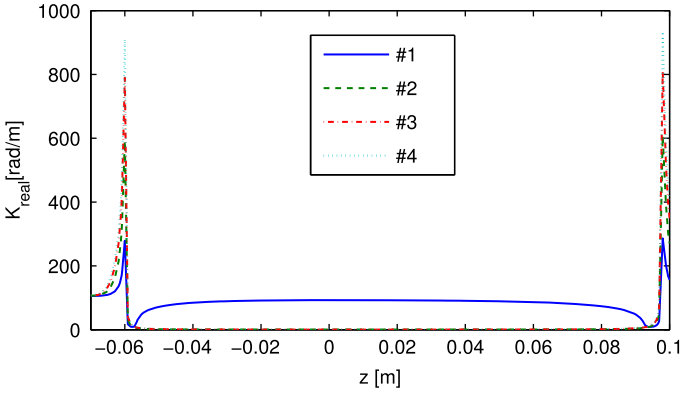

Figure 15. Propagation constant k_{real} (rad/m) along longitudinal z-axis.

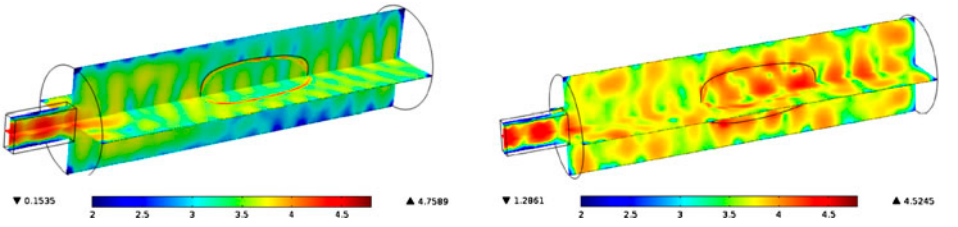

(a) $\log_{10}(|E|+1)$: Electric fied on multislice with # 1 density profile

(b) $\log_{10}(|E|+1)$: Electric fied on multislice with # 3 density profile

Figure 16. Electric field at two different density profiles.

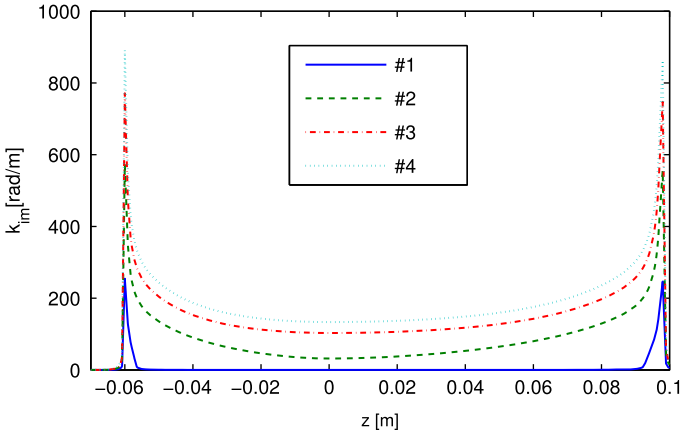

Figure 17. Attenuation constant along longitudinal z-axis.

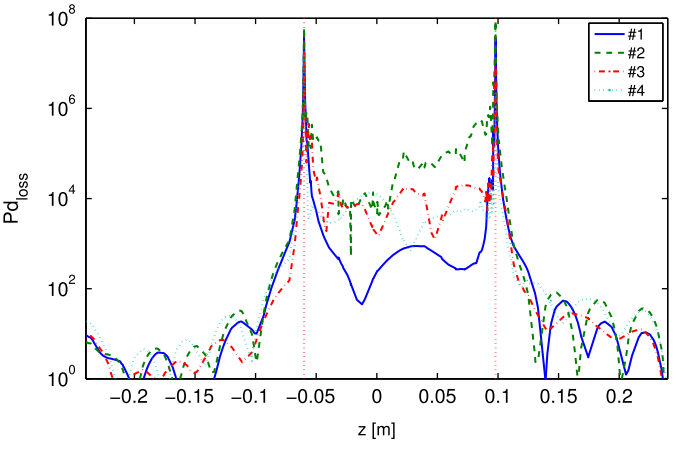

Figure 18. Power loss density Pd_{loss} over z-axis. At ECR layers(red dot lines) Pd_{loss} show a maximum.

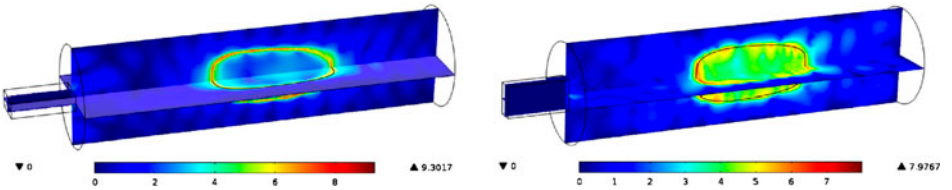

(a) Power loss density with # 1 density profile (b) Power loss density with # 3 density profile

Figure 19. Electromagnetic power loss density (W/m^3) (logarithmic scale).

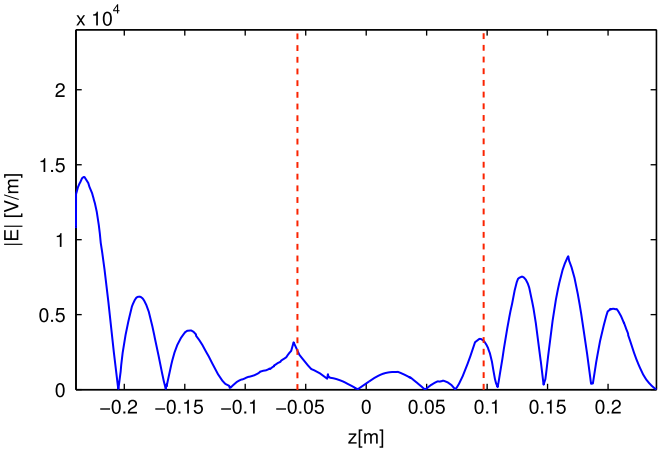

Figure 20. Oversimplified model: electric field along z-axis. The red-dashed lines highlight the ECR layer positions.

Table 3. Summary of simulation results at 5 GHz.

Simulation setup	P_{loss} (W)	E_{max} (V/m)
#1	72.9	6.3e5
#2	79	2.9e5
#3	39.3	4e5
#4	35.5	2.5e4

(Figure 15) becomes very small, producing a greater discontinuity of the propagation constant from inside to outside the plasmoid.

The cavity effect provided by the plasma, producing the mentioned field amplification, is more evident by looking Figure 16: it compares 3D electric field distribution for low-density (#1) and quasi-critical plasma-density (#3) condition. Increasing the plasma density, both Figures 17 and 18 show that the inner plasmoid electromagnetic loss power increases (Figure 19). The case #4, showing a propagating mode also inside the plasmoid, confirms that a restrictive plane wave analysis [9] is not feasible in ECRIS-like configuration. As a feedback in Figure 20, the pure damping effect inside an overdense plasmoid considering the restrictive simplified model of an equivalent O-wave refractive index is shown.

In Table 3, some important simulation results are listed as a summary of the analysis described. It demonstrates how strong is the effect of the plasma load on coupling properties.

4. Conclusion

In this paper, we have developed an electromagnetic model of an ECRIS plasma in order to perform 3D full-wave FEM simulations of the electromagnetic field in propagation. For the first time, 3D simulations considering a non-uniform magnetized plasma complex dielectric tensor have been implemented and solved with realistic boundaries condition in an anisotropic medium. The model optimally considers plasma effects on cavity mode structures and losses by cavity walls and the effect of wave absorption by the lossy plasma. These simulations are an important step forward because wave equation and dispersion relation are not approximated by pre-setting any a priori magnitude and direction of the wave vector nor considering an equivalent media modeling the plasma load. The general approach has allowed a systematic study by using different initial parameters in terms of density distribution. The simulations show that the propagation is strongly influenced by the density profile especially close to ECR positions. In addition, the tensor-based simulations differ considerably from outputs based on single-mode propagation, meaning that modal conversion and cavity wall effects cannot be neglected when investigating electromagnetic field propagation in ECRIS. In the perspective of ECRIS science and technology studies, these simulations represent a crucial step towards self-consistent modeling of wave-to-electron interaction dynamics. It is expected that a predictive approach can be based on these first results, helping in the design of future machines (especially the plasma chamber) optimized for high wave damping at ECR layer, low reflected power, efficient electron heating producing a dense plasma, and high current beam of multicharged ions. The approach, however, is general and can be easily extended to similar plasma devices fed by microwave in the GHz range. The next step will be the implementation of the hot plasma dielectric tensor effects that play an important role in ECRIS plasma dynamics.

Acknowledgements

The authors are warmly grateful to the INFN V Nat. Sci. Commission funding the RDH-UTOPIA project.

Notes

1. Cold plasma approximation assumes that the electron temperature is relatively smaller than wave's phase velocity ($v_{th} \gg v_\phi$). It is traditionally assumed: $T_e = T_i \cong 0$. For more details, see [8].
2. High computational costs of the FEM simulations for large problems with high frequency lead us to consider a slightly lower frequency (8 GHz however), as a first step, with respect to the typical operational frequencies ($\nu_{RF} > 10$ GHz) of second-generation ECRIS. We chose this frequency value, much higher than the fundamental resonant frequency of the empty cavity, to be sure that we have enough degree of freedoms to excite an electromagnetic field distribution pattern with a large azimuthal and longitudinal mode number.
3. This number refers to the minimum mesh density outside the ECR critical surface.
4. That is traditionally called "overdense" plasma condition in which, the upper limit of density n_c, allowing field propagation in ECRIS plasmas, is overcome.

References

[1] Ropponen T, Tarvainen O, Suominen P, Koponen TK, Kalvas T, Koivisto H. Hybrid simulation of electron cyclotron resonance heating. Nucl. Instrum. Methods Phys. Res. A. 2008;587: 115–124.

[2] Geller R. Electron cyclotron resonance ion sources and ECR plasmas. London: Institute of Physics; 1996.
[3] Celona L, Gammino S, Ciavola G, Maimone F, Mascali D. Microwave to plasma coupling in electron cyclotron resonance and microwave ion sources. Rev. Sci. Instrum. 2010;81:02A333.
[4] Mascali D, Neri L, Gammino S, Celona L, Ciavola G, Gambino N, Miracoli R, Chikin S. Plasma ion dynamics and beam formation in electron cyclotron resonance ion sources. Rev. Sci. Instrum. 2010;81:2–4.
[5] Celona L, Ciavola G, Consoli F, Gammino S, Maimone F, Mascali D, Spädtke P, Tinschert K, Lang R, Mäder J, Robbach J, Barbarino S, Catalano RS. Observations of the frequency tuning effect in the 14GHz CAPRICE ion source. Rev. Sci. Instrum. 2008;79:023305.
[6] Crombe K, Kyrytsya V, Koch R, Van Eester D. Simulations of ICRF antenna nearfields in dielectric media and cold plasmas with COMSOL. AIP Conf. Proc. 2011;1406:97–100.
[7] El Khaldi M, Milanesio D, Maggiora R, Magne R, Vulliez K. Electromagnetic modelling of dielectric loads in front of an ICRH ITER array using TOPICA and HFSS codes for comparison. AIP Conf. Proc. 2009;1187:273–276.
[8] Stix TH. Waves in plasmas. New York (NY): AIP; 1992.
[9] Clugghish BP, Kim JS. Modeling of wave propagation and absorption in electron cyclotron resonance ion source plasmas. Nucl. Instrum. Methods Phys. Res. A. 2012;664:84–97.
[10] Swanson DG. Plasma waves. San Diego (CA): Academic Press; 1989.
[11] RF Module Users Guide COMSOL Multiphysics. 4.3b.
[12] Mascali D, Gammino S, Celona L, Ciavola G. Towards a better comprehension of plasma formation and heating in high performances electron cyclotron resonance ion sources. Rev. Sci. Instrum. 2012;83:02A336.
[13] MUMPS: a MUltifrontal Massively Parallel sparse direct Solver. Available from: http://mumps.enseeiht.fr.
[14] Toivanen V, Koivisto H, Steczkiewicz O, Celona L, Tarvainen O, Ropponen T, Gammino S, Mascali D, Ciavola G. Effect of electron cyclotron resonance ion source frequency tuning on ion beam intensity and quality at Department of Physics, University of Jyvaskyla. Rev. Sci. Instrum. 2010;81:02A319.